NUCLEAR SCIENCE AND TECHNIQUES **25**, 050303 (2014)

Preparation and characterization of the antifouling porous membranes from poly(vinylidene fluoride)-graft-poly(*N*-vinyl pyrrolidone) powders*

CHEN Li-Fang (陈利芳),[1,2] BIAN Xiao-Kai (卞晓锴),[1] HOU Zheng-Chi (侯铮迟),[1]
LIU Zhong-Ying (刘忠英),[1] QIN Qiang (秦强),[1] PAN Ling (潘玲),[1,2]
SHEN Li-Guo (申利国),[1] SHI Liu-Qing (施柳青),[1,2] and LU Xiao-Feng (陆晓峰)[1,†]

[1] *Shanghai Institute of Applied Physics, Chinese Academy of Sciences, Jiading campus, Shanghai 201800, China*
[2] *University of Chinese Academy of Sciences, Beijing 100049, China*

(Received February 17, 2014; accepted in revised form May 12, 2014; published online October 6, 2014)

Porous membranes were prepared using the phase inversion method from poly(vinylidene fluoride)-graft-poly(*N*-vinyl pyrrolidone) (PVDF-*g*-PVP) powders, which were synthesized via γ-ray induced graft polymerization (pre-irradiation). Chemical compositions, thermal behavior, morphology and hydrophilicity of the membranes were characterized by Fourier transform infrared spectroscopy, X-ray photoelectron spectroscopy, element analysis, thermalgravimetric analysis, differential scanning calorimetry, scanning electron microscopy and contact angle measurements, respectively. Permeation experiments were conducted to evaluate the water flux, and the dynamic BSA fouling resistance performances were investigated, too. All the experimental results indicate that the PVDF-*g*-PVP membranes demonstrate better separation performances over the pristine PVDF membrane.

Keywords: Poly(vinylidene fluoride)-graft-poly(*N*-vinyl pyrrolidone), Porous membrane, Characterization

DOI: 10.13538/j.1001-8042/nst.25.050303

I. INTRODUCTION

Poly(vinylidene fluoride) (PVDF) membranes are widely used in microfiltration and ultrafiltration processes due to their good thermal stability, chemical resistance, ultraviolet and radiation resistance, and well-controlled porosity [1–4]. Yet, because of the hydrophobic nature of PVDF, protein fouling often occurs both on the membrane surface and within the pores when the membranes are exposed to protein containing solutions, which, in turn, restricts the applications of PVDF membranes [5, 6]. In recent years, membrane researchers have attempted to improve hydrophilicity of PVDF membranes using grafting methods, such as surface living/controlled radical polymerization [7–9], plasma-induced grafting [10–12], UV-assisted graft polymerization [13–16], and radiation-induced graft polymerization [17–21]. Hydrophilic functional monomers are grafted onto PVDF main chains or membrane surfaces with the grafting methods. But by grafting the membrane surface directly, the membrane pore size and distribution can be changed, hence the reduction of permeability [22, 23].

In this study, we proposed a routine of graft polymerization of PVDF powders by ^{60}Co γ-ray pre-irradiation to fabricate porous membranes. The radicals formed in PVDF powders by γ-rays initiate the graft polymerization of vinyl monomers, and functional graft chains are introduced to endow PVDF with desirable properties [24–26]. In our previous work, hydrophilic poly(vinylidene fluoride)-graft-poly(*N*-vinyl pyrrolidone) (PVDF-*g*-PVP) powders were prepared by grafting *N*-vinyl pyrrolidone (NVP) onto PVDF powders using the pre-irradiation method [27]. In this paper, the porous membranes are cast from PVDF-*g*-PVP powders of different degrees of grafting (*DG*) via the phase inversion method. The chemical compositions, thermal behavior, morphology, hydrophilicity and water flux of the membranes are investigated, and antifouling property of the porous membranes is examined.

II. EXPERIMENTAL

A. Materials

PVDF powders (TA-6020) were purchased from Solvay Co. Ltd. (Brussels, Belgium). NVP of analytical grade was obtained from J&K Corp. (Shanghai, China). *N*-methyl pyrrolidone (NMP), hydrochloric acid of analytical grade, bovine serum albumin (BSA, $Mw = 67\,000$ Da) and phosphate-buffered saline (PBS) were purchased from Sinopharm Reagent Co. Ltd. (Shanghai, China). All the materials were used without further purification.

B. Membrane preparation

The porous membranes were prepared using the immersion precipitation phase inversion method. PVDF and PVDF-*g*-PVP powders of different *DG*s were dissolved in NMP ($wt\% = 16\%$) at 70 °C for 7 days to obtain a homogenous solution. The solution was casted onto a glass plate at (24 ± 1) °C, which was then immersed in a precipitation bath of deionized water maintained at (16 ± 1) °C. The new-born membrane was evaporated in air for 20 s. The prepared membranes were immersed into fresh deionized water to remove all the residual solvent before their characterizations.

* Supported by the Shanghai Municipal Science and Technology Committee (No. 08231200300)
† Corresponding author, luxiaofeng@sinap.ac.cn

C. Membrane characterization

1. *Fourier transform infrared (FTIR) spectroscopy measurements*

The FTIR spectra were recorded on a TENSOR 27 FTIR spectrometer (Bruker Optics, Germany) in attenuated total reflection (ATR) mode. The samples were placed on the sample holder and all spectra were recorded in the wavenumber range of 4000–600 cm^{-1} by cumulating 32 scans at a resolution of 4 cm^{-1}.

2. *X-ray photoelectron spectroscopy (XPS) analysis*

XPS analysis was performed with a Kratos Axis Ultra DLD XPS instrument (Kratas Analytical Ltd., Manchester, UK) equipped with a monochromatized Al K_α X-ray source at a constant dwelling time of 100 ms and a pass energy of 160 eV. The samples were vacuum-dried before measurement. Peak analysis software was applied to analyze the spectra.

3. *Elemental analysis*

The bulk C, H and N contents of the membranes were determined on a Vario EL III elemental analyzer (Elementar Co., Hanau, Germany). Each membrane was measured twice.

4. *Thermal behavior analysis*

Thermalgravimetric analysis (TGA) was performed on a Pyris1 TGA thermogravimetric analyzer (Perkin Elmer, USA) between 50 °C and 800 °C. The samples were heated from 50 °C to 100 °C at a rate of 40 °C/min. In order to eliminate the influence of adsorbed water, all the samples were kept at 100 °C for 5 min before they were heated to 800 °C at a rate of 10 °C/min, for their test in an alumina crucible under nitrogen purging at 20 mL/min.

Differential scanning calorimetry (DSC) analysis was performed on a METTLER TOLEDO DSC822e DSC instrument (Mettler-Toledo International Inc., Zurich, Switzerland) at 25–250 °C in a heating rate of 10 °C/min under nitrogen gas atmosphere. To eliminate thermal history of the samples, scans were taken twice, and the second scan results were recorded.

5. *Scanning electron microscope (SEM) analysis*

Morphology of the porous membranes was studied on an LEO1530vp SEM (Zeiss, Germany). To obtain the cross-section images, the membranes were immersed in liquid nitrogen and fractured. The samples were attached on a carbon tape, coated with Au by sputtering, and scanned at 25 kV and 10 mA.

6. *Contact angle measurements*

Contact angles of the membranes were measured on an Attension Theta system (KSV Instruments Ltd., Finland). A water drop (5.0 μL) was lowered onto the membrane surface from a needle tip. A magnified image of the droplet was recorded with a digital camera. Static contact angles were calculated from the images with a software, and measurements at six points of a membrane were averaged as its contact angle.

7. *Water flux measurements*

A self-made microfiltration cell apparatus [28] with an effective filtration area of 0.002 m^2 was used to measure the flux of the membranes. A sample membrane was mounted onto the filtration cell and pre-compacted at −10 kPa for a certain time until the flux maintained a constant value. The flux (J) was calculated by $J = V/(A \cdot \Delta T)$, where V is the volume of permeation water, A is effective area of the membrane, and ΔT is the time of measurement.

8. *Evaluation of antifouling property*

BSA was chosen as the model protein to evaluate the antifouling property of the membranes. After the water flux measurement, pure water was changed to 1 g/L BSA solution in PBS (pH = 7.4). The sample membrane was kept filtering for 4 h with BSA solution under stirring. And the permeate flux profile with time was recorded to determine the fouling resistance of the membrane. Filtration runs were performed with full recycle of penetrant to the feed tank to maintain the BSA concentration at a constant level.

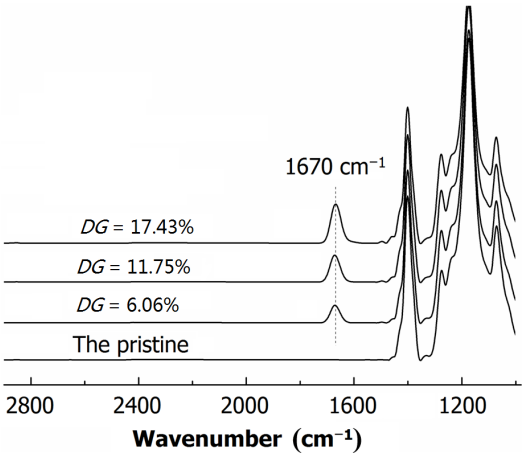

Fig. 1. FTIR-ATR spectra of PVDF-*g*-PVP membranes of different DGs.

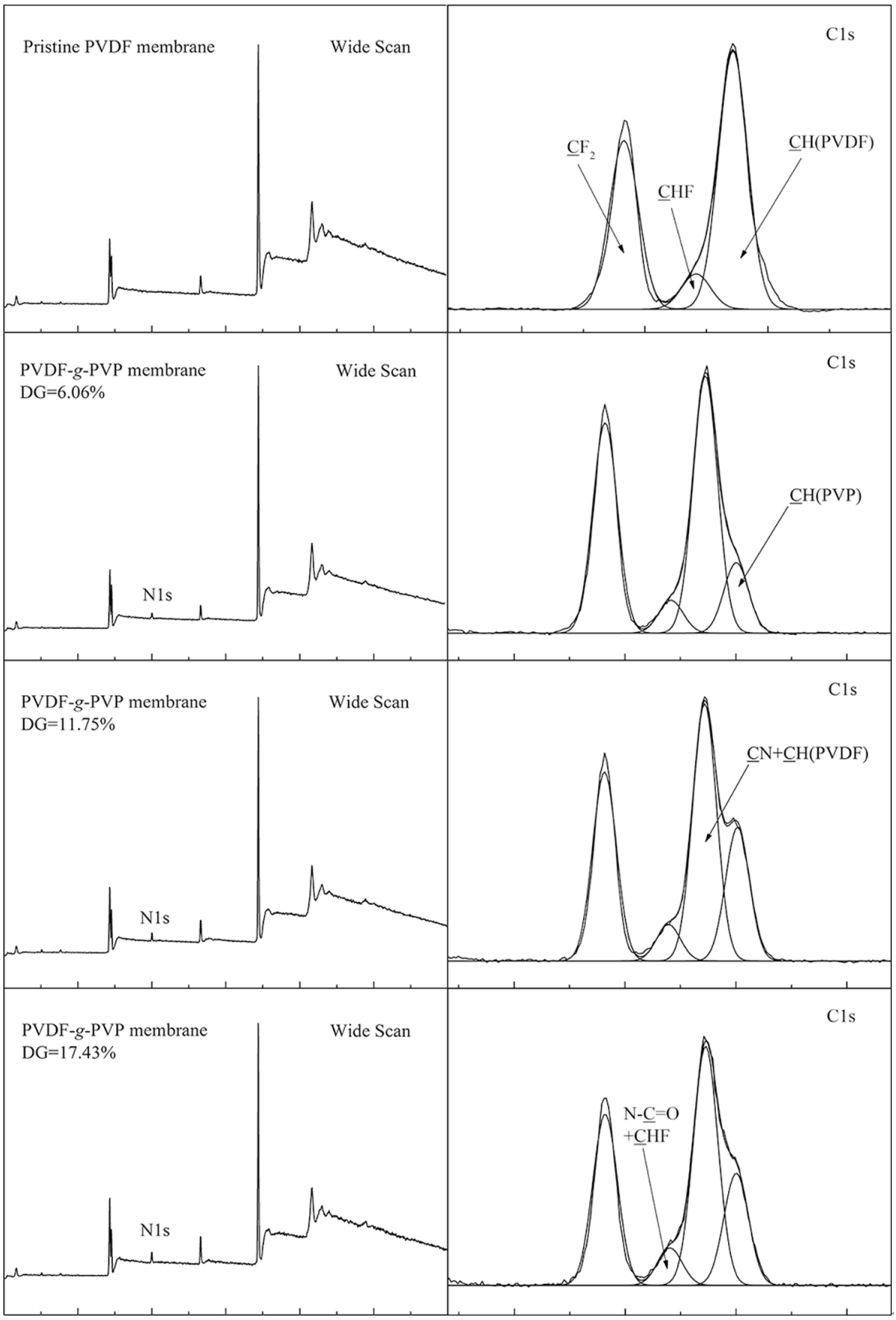

Fig. 2. XPS wide-scan and C1s core-level spectra of PVDF-*g*-PVP membranes of different *DG*s.

III. RESULTS AND DISCUSSION

A. FTIR-ATR spectroscopy

FTIR-ATR spectra of pristine PVDF membrane and PVDF-*g*-PVP membranes with different *DG*s are compared in Fig. 1. A distinctive new band around 1670 cm^{-1} can be seen in the spectra of PVDF-*g*-PVP membranes, and the absorbance increases with *DG*. This band is from characteristic vibrations attributing to C=O stretching in the grafted PVP chains. The results confirmed the existence of PVP chains on PVDF-*g*-PVP membrane surface.

B. XPS analysis

Surface compositions of the PVDF-*g*-PVP membranes were studied by XPS. Fig. 2 shows the wide-scan and C1s core-level spectra of the porous membranes. The wide-scan spectra have signals attributed to C, F and O elements in the PVDF-*g*-PVP membranes, and the new signal at 399.8 eV is attributed to the N element originating from the amide groups in PVP polymer chains. The minuscule amount of O element in PVDF powders may be due to the remaining initiator and surfactant, but the supplier did not provide any information on these details.

In the C1s core-level spectrum of the pristine PVDF membrane, the peaks at 286.4 eV and 290.8 eV represent CH_2 and CF_2 species, respectively, and the peak at 287.9 eV is of the CHF species. For the PVDF-*g*-PVP membranes, three new peak components appeared in the C1s core-level spectra, which are assigned to the grafted PVP polymer chains, involving BEs at 287.9 eV for the N-C-O species, at 284.9 eV for the hydrocarbon of the PVP chains, and at 286.4 eV for the CN species. The CN and (CH_2) (PVDF) peaks overlap to form a single peak in Fig. 2, and so do the CHF and N-C-O peaks.

TABLE 1. Elemental contents (in percentage) of PVDF-*g*-PVP membranes of different *DG*s

Membrane	C_{bulk}(%)	H_{bulk}(%)	N_{bulk}(%)	$N_{surface}$(%)
The pristine	37.63	3.22	—	—
$DG = 6.06\%$	38.66	3.46	0.75	1.54
$DG = 11.75\%$	38.93	3.55	0.95	2.09
$DG = 17.43\%$	39.44	3.68	1.23	2.44

C. Elemental analysis

The C, H and N contents of the PVDF-*g*-PVP membranes are listed in Table 1. The bulk C, H and N contents were determined by elemental analysis, and the surface N contents were calculated from XPS spectra. From Table 1, the bulk and surface N contents increase with *DG*, and the surface N content of each grafted membrane is much higher than the corresponding bulk N content. That is to say, the PVP polymer concentration of the membrane surface is higher than that of the membrane bulk. This is attributed to surface segregation of the hydrophilic PVP graft chains during membrane fabrication by the phase inversion in the aqueous medium, due to the relatively-low interfacial energy between the PVP graft chains and water [29–31].

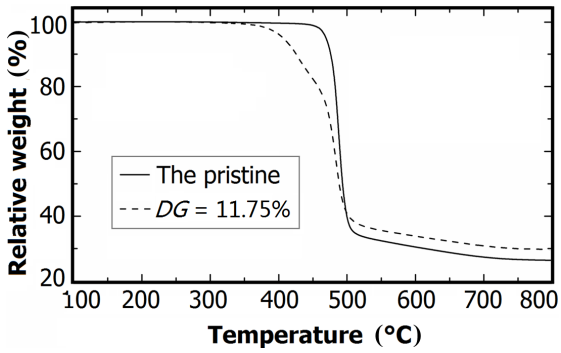

Fig. 3. TGA curves of pristine and grafted ($DG = 11.75\%$) PVDF membranes.

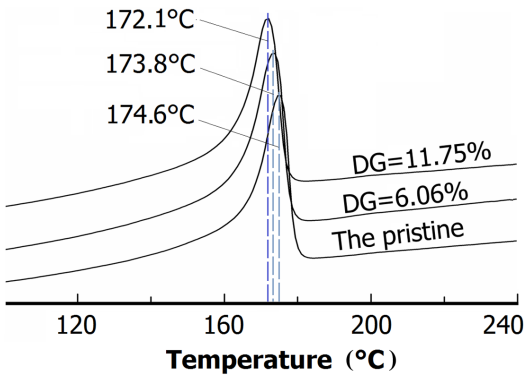

Fig. 4. (Color online) DSC curves of the pristine and grafted PVDF membranes.

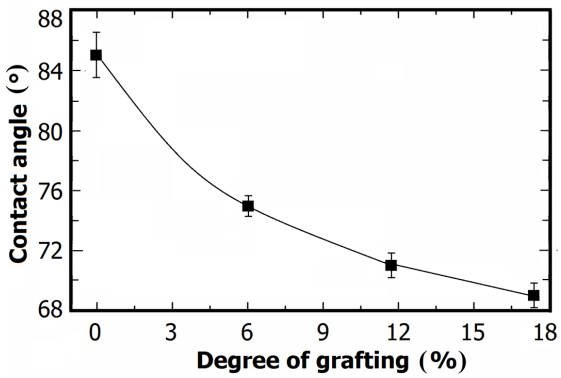

Fig. 5. Contact angles of porous membranes as a function of *DG*.

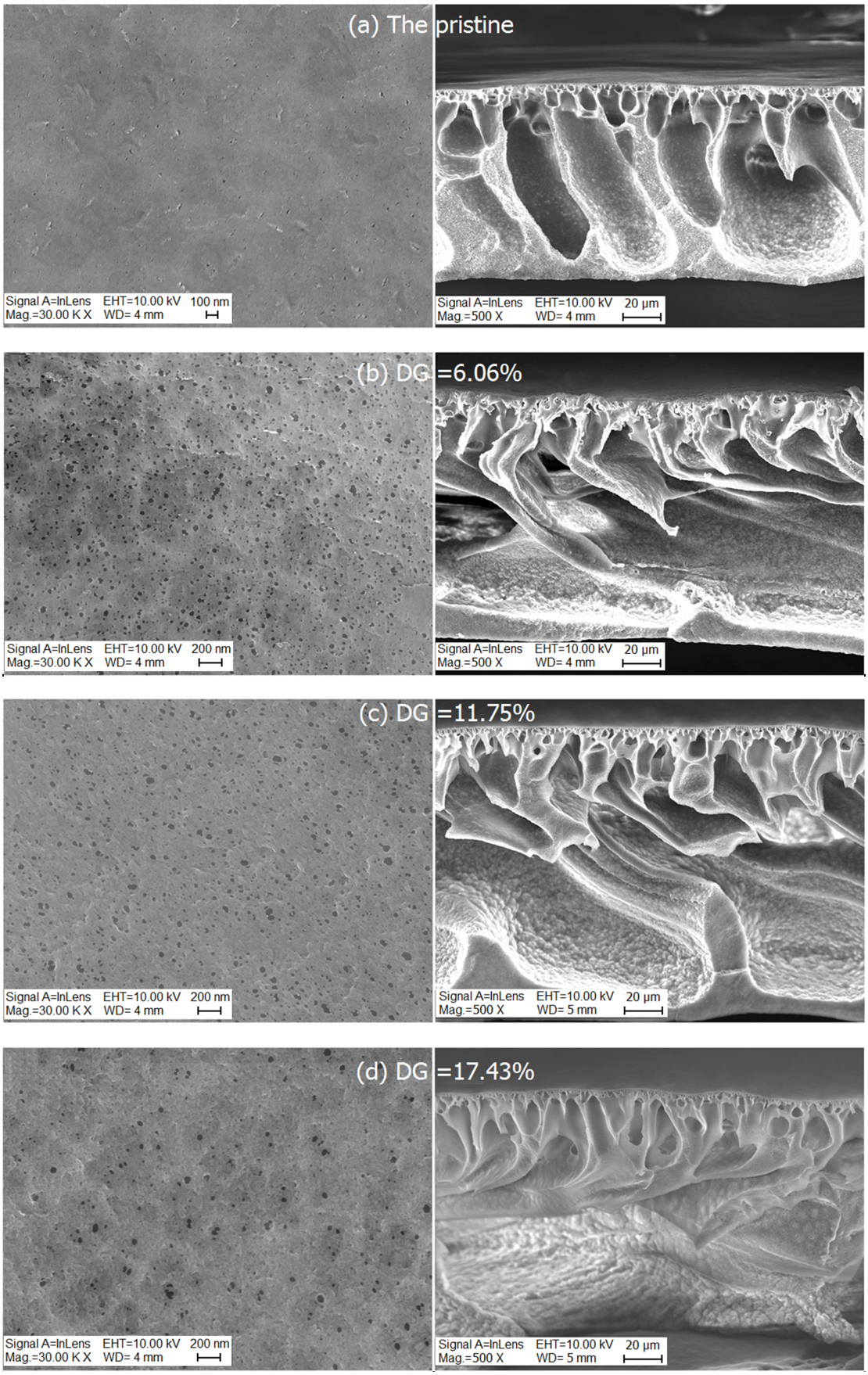

Fig. 6. Surface (left) and cross-section (right) SEM images of the pristine and grafted PVDF membrane.

D. Thermal behavior analysis

Thermal behavior of the porous membranes was investigated by TGA and DSC measurements. Fig. 3 shows the TGA curves of two PVDF membranes. The pristine PVDF membrane has only one thermal decomposition step, commencing at about 460 °C, while the PVDF-*g*-PVP membrane ($DG = 11.75\%$) exhibits a two-step thermal decomposition process. The first main weight loss starting at about 340 °C is attributed to degradation of the PVP side chains, while the second weight loss beginning at about 460 °C is attributed to decomposition of the PVDF main chains. The two-step decomposition of PVDF-*g*-PVP membranes suggests that the PVP grafts do not alter the inherent decomposition of the matrix PVDF.

Figure 4 shows the DSC curves of PVDF-*g*-PVP membranes of different *DG*s. Melting temperature of the porous membranes decreased slightly with increasing *DG*s, being 174.6 °C for the pristine PVDF membrane but 173.8 °C and 172.1 °C for the grafted membranes of $DG = 6.06\%$ and $DG = 11.75\%$, respectively. This is because that the proportion of PVP increases with *DG*, and PVP is of lower melting temperature than PVDF.

E. Surface hydrophilicity analysis

Surface hydrophilicity of the membranes was obtained by contact angle measurement (Fig. 5). Contact angle of the pristine PVDF membrane is 85° because of the intrinsic hydrophobicity of PVDF. Due to the existence of carbonyl groups in the PVP chains, the grafted membranes are relatively hydrophilic, and the contact angles decrease with increasing DGs, being 69° at $DG = 17.43\%$. So, hydrophilicity of PVDF-*g*-PVP membranes is obviously improved.

F. Morphology study

SEM images of the pristine and grafted PVDF membranes of different *DG*s are shown in Fig. 6. From the surface images, one sees that the number of pores in PVDF-*g*-PVP membranes are evidently greater than that of the pristine membrane. The pore sizes of PVDF-*g*-PVP membranes are larger than those of the pristine. This is due to the enhanced hydrophilicity of PVDF-*g*-PVP powders, which is beneficial for the pore forming during the membrane fabrication process. However, when *DG* is higher, the number of pores decreases, especially the pores of smaller size. The grafted PVP chains may plug or cover the membrane pores, resulting in decreased surface porosity [1, 32]. As evident from the cross-section SEM images, an asymmetric morphology with a skin layer and macrovoids in the support layer can be observed for both the pristine and grafted membranes. However, the pore connectivity of PVDF-*g*-PVP membranes is greater than that of the pristine. Thickness of PVDF-*g*-PVP membranes changed a little from that of the pristine. This change may be due to a variable exchange rate between water and the solvent [33]. Also, the angle from which the SEM image was taken may cause a difference in the membrane thickness.

G. Water flux

Figure 7 shows the water flux of the porous membranes as a function of *DG*. The water flux of PVDF-*g*-PVP membranes is higher than that of the pristine, but it decreases with increasing *DG*s, being 79.91 L/(m^2 h) at $DG = 6.06\%$ while just 18.14 L/(m^2 h) at $DG = 7.43\%$. In general, the water flux of membranes is mainly controlled by the membrane hydrophilicity and the membrane structure. With improved hydrophilicity, a greater number of pores of larger pore size are beneficial to the improvement in flux [28]. Although the hydrophilicity of PVDF-*g*-PVP membranes increases with *DG* based on the contact angle results, the surface SEM images show that the porosity of the grafted membranes reduces with increasing *DG*. Obviously, the membrane structure influences the water flux significantly in this case. Consequently, the water flux of PVDF-*g*-PVP membranes decrease with increasing *DG*.

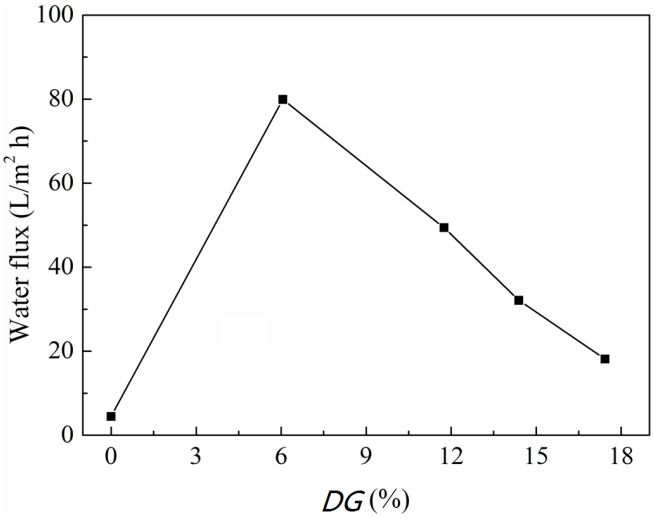

Fig. 7. Water flux of porous membranes as a function of *DG*.

H. Antifouling property analysis

Antifouling behavior of the porous membranes was investigated with respect to dynamic BSA fouling. The results in terms of permeate flux relative to pure water flux are shown in Fig. 8. It can be seen that both the pristine and grafted membranes exhibit a flux decline resulting from fouling. In comparison, the flux decline of PVDF-*g*-PVP membranes is rather mild. For example, after 4 h of continuous filtration, the flux of the pristine and PVDF-*g*-PVP membrane of $DG = 11.75\%$ dropped to 52.78% and 82.54% of its initial pure water flux, respectively, indicating improved antifouling property of the

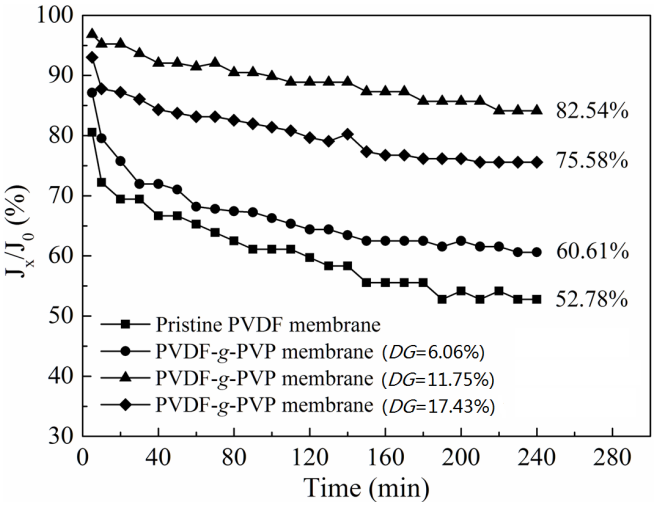

Fig. 8. Normalized flux of PVDF-*g*-PVP membranes of different *DG*s in 4 h filtration of 1 g/L BSA solution.

grafted PVDF membrane. However, the flux of the PVDF-*g*-PVP membrane of $DG = 17.43\%$ dropped to 75.58% of its initial pure water flux, which is lower than that of the PVDF-*g*-PVP membrane of $DG = 11.75\%$. Both hydrophilicity and pore size distribution will affect the BSA fouling on the membrane surface [7, 34–36]. The PVDF-*g*-PVP membrane of $DG = 17.43\%$ shows the highest hydrophilicity and should exhibit the best antifouling property. However, its mean pore size is the largest of all the porous membranes, which can influence the fouling resistance significantly. Considering the two factors, the PVDF-*g*-PVP membrane of $DG = 11.75\%$ exhibits the best antifouling property.

IV. CONCLUSION

The porous membranes were cast from pristine PVDF and PVDF-*g*-PVP powders with different *DG*s by the phase inversion method. The existence of PVP graft chains in PVDF-*g*-PVP membranes has been demonstrated by FTIR-ATR and XPS spectroscopy. The hydrophilicity of PVDF-*g*-PVP membranes was improved compared to the pristine PVDF membrane, due to the existence of the hydrophilic PVP graft chains, which consequently led to a reduced contact angle. Furthermore, the hydrophilicity of PVDF-*g*-PVP membranes was intensified with increasing *DG*. The different PVP polymer concentration in the membrane bulk and on the membrane surface confirmed surface segregation of the hydrophilic PVP polymer in the surface region. Thermal behavior analysis showed that the PVDF-*g*-PVP membranes exhibited a two-step thermal decomposition process, and the melting temperature of PVDF-*g*-PVP membranes was decreased slightly than the pristine one. SEM images demonstrated that the PVDF-*g*-PVP membrane with a *DG* of 6.06% exhibited the greatest porosity, which led to the highest water flux, and the pore connectivity of PVDF-*g*-PVP membranes was greater than that of the pristine PVDF membrane. Filtration performance evaluation indicated that the PVDF-*g*-PVP membranes had better fouling resistance than the pristine one, and the PVDF-*g*-PVP membrane with a *DG* of 11.75% exhibited the best antifouling property.

[1] Wang D L, Li K, Teo W K. J Membrane Sci, 1999, **163**: 211–220.
[2] Dargaville T R, George G A, Hill D J T, *et al*. Prog Polym Sci, 2003, **28**: 1355–1376.
[3] Chiang Y, Chang Y, Higuchi A, *et al*. J Membrane Sci, 2009, **339**: 151–159.
[4] Su Y L, Liang Y G, Mu C X, *et al*. Ind Eng Chem Res, 2011, **50**: 10525–10532.
[5] Krishnan S, Weinman C J, Ober C K. J Mater Chem, 2008, **18**: 3405–3413.
[6] Wang P, Tan K L, Kang E T, *et al*. J Membrane Sci, 2002, **195**: 103–114.
[7] Zhai G Q, Kang E T, Neoh K G. Macromolecules, 2004, **37**: 7240–7249.
[8] Singh N, Husson S M, Zdyrko B, *et al*. J Membrane Sci, 2005, **262**: 81–90.
[9] Chen Y W, Deng Q, Xiao J C, *et al*. Polymer, 2007, **48**: 7604–7613.
[10] Kaur S, Ma Z W, Gopal R, *et al*. Langmuir, 2007, **23**: 13085–13092.
[11] Park Y W, Inagaki N. Polymer, 2003, **44**: 1569–1575.
[12] Duca M D, Plosceanu C L, Pop T. Polym Degrad Stabil, 1998, **61**: 65–72.
[13] Taniguchi M, Belfort G. J Membrane Sci, 2004, **231**: 147–157.
[14] Wu G G, Li Y P, Han M, *et al*. J Membrane Sci, 2006, **283**: 13–20.
[15] Asano M, Chen J, Maekawa Y, *et al*. J Polym Sci A1, 2007, **45**: 2624–2637.
[16] Rahimpour A, Madaeni S S, Zereshki S, *et al*. Appl Surf Sci, 2009, **255**: 7455–7461.
[17] Deng B, Yu Y, Zhang B W, *et al*. Radiat Phys Chem, 2011, **80**: 159–163.
[18] Yang X X, Zhang B W, Liu Z Y, *et al*. J Mater Chem, 2011, **21**: 11908–11915.
[19] Liu F, Du C H, Zhu B K, *et al*. Polymer, 2007, **48**: 2910–2918.
[20] Betz N, Begue J, Goncalves M, *et al*. Nucl Instrum Meth B, 2003, **208**: 434–441.
[21] Yang X X, Deng B, Liu Z Y, *et al*. J Membrane Sci, 2010, **362**: 298–305.
[22] Kaeselev B, Pieracci J, Belfort G. J Membrane Sci, 2001, **194**: 245–261.
[23] Shi Q, Su Y L, Zhu S P, *et al*. J Membrane Sci, 2007, **303**: 204–212.
[24] Ying L, Wang P, Kang E T, *et al*. Macromolecules, 2002, **35**: 673–679.
[25] Ying L, Zhai G, Winata A Y, *et al*. J Colloid Interf Sci, 2003, **265**: 396–403.

[26] Zhai G, Kang E T, Neoh K G. J Membrane Sci, 2003, **217**: 243–259.
[27] Chen L F, Hou Z C, Lu X F, *et al*. J Appl Polym Sci, 2013, **128**: 3949–3956.
[28] Deng B, Yang X X, Xie L D, *et al*. J Membrane Sci, 2009, **330**: 363–368.
[29] Hester J F and Mayes A M. J Membrane Sci, 2002, **202**: 119–135.
[30] Bousquet A, Ibarboure E, Labrugere C, *et al*. Langmuir, 2007, **23**: 6879–6882.
[31] Asatekin A, Menniti A, Kang S, *et al*. J Membrane Sci, 2006, **285**: 81–89.
[32] Zhang M, Nguyen Q T, Ping Z. J Membrane Sci, 2009, **327**: 78–86.
[33] Shen L G, Bian X K, Lu X F, *et al*. Desalination, 2012, **293**: 21–29.
[34] Liu F, Moghareh A M R, Li K. J Membrane Sci, 2011, **366**: 97–103.
[35] Ying L, Kang E T, Neoh K G. J Membrane Sci, 2002, **208**: 361–374.
[36] Chang Y, Shih Y J, Ruaan R C, *et al*. J Membrane Sci, 2008, **309**: 165–174.